

MMLGNet: Cross-Modal Alignment of Remote Sensing Data using CLIP

Aditya Chaudhary  Sneha Barman  Mainak Singha 
Dept. of CSE *DAGP* *CSRE*
 The LNMIIT Jaipur IIT Dhanbad IIT Bombay

Ankit Jha  Girish Mishra  Biplob Banerjee 
Dept. of CSE *SAG* *CSRE*
 The LNMIIT Jaipur DRDO, Delhi IIT Bombay

Abstract

In this paper, we propose a novel multimodal framework, Multimodal Language-Guided Network (MMLGNet), to align heterogeneous remote sensing modalities like Hyperspectral Imaging (HSI) and LiDAR with natural language semantics using vision-language models such as CLIP. With the increasing availability of multimodal Earth observation data, there is a growing need for methods that effectively fuse spectral, spatial, and geometric information while enabling semantic-level understanding. MMLGNet employs modality-specific encoders and aligns visual features with handcrafted textual embeddings in a shared latent space via bi-directional contrastive learning. Inspired by CLIP’s training paradigm, our approach bridges the gap between high-dimensional remote sensing data and language-guided interpretation. Notably, MMLGNet achieves strong performance with simple CNN-based encoders, outperforming several established multimodal visual-only methods on two benchmark datasets, demonstrating the significant benefit of language supervision. Codes are available at https://github.com/AdityaChaudhary2913/CLIP_HSI.

Index Terms—Hyperspectral image classification, multimodal learning, CLIP

I. INTRODUCTION

Remote sensing systems increasingly rely on a diverse set of sensors such as Hyperspectral Imaging (HSI), Multispectral Imaging (MSI), and Light Detection and Ranging (LiDAR), each offering unique advantages in characterizing the Earth’s surface. HSI provides fine spectral granularity, enabling material discrimination [1]; MSI offers broader spectral coverage with fewer channels and higher spatial resolution; and LiDAR contributes structural and topographic information [2]. The fusion of these modalities has shown promise in tasks like land use mapping [3], crop type classification [4], and environmental monitoring [5, 6]. Despite these benefits, combining such heterogeneous data sources presents non-trivial challenges, primarily due to differences in spatial resolution, modality-specific noise, and limited availability of aligned datasets. Traditional fusion approaches such as pixel-level stacking [7], feature concatenation [8, 9], or decision-level [10] voting suffer from scalability issues and often demand extensive labeled data for supervised learning.

Recent advances in vision-language pretraining, particularly Contrastive Language Image Pretraining (CLIP) [11], have opened a new direction: using textual supervision as a unifying

modality to encode visual content semantically. CLIP aligns images and text in a shared embedding space via contrastive learning, allowing zero-shot recognition based on class names or textual prompts. Although widely successful on natural image datasets like ImageNet [12], CLIP and its adaptations have yet to be deeply explored in the context of multimodal remote sensing data. Several efforts have extended CLIP-like architectures to overhead imagery focusing primarily on RGB data [13]. However, such methods generally overlook richer modalities like HSI and LiDAR, which offer deeper spectral or structural cues critical for fine-grained semantic understanding. Work like GeoCLIP [14] attempted to incorporate geospatial knowledge into language-image models, but their focus remained on natural color or pseudo-color imagery. Additionally, while a few studies have explored integrating HSI with deep learning for classification, and even fewer have considered language supervision, there is a clear research gap in unifying diverse remote sensing modalities under a vision-language framework.

In this paper, we propose MMLGNet a simple framework for aligning multimodal remote sensing data with CLIP. It leverages contrastive pretraining to bridge HSI, and LiDAR data with natural language descriptions. The core objective is to align visual features from different modalities with textual embeddings, enabling the learning of robust representations in a shared latent space. We design modality-specific encoders that preserve spectral, spatial, and structural information, followed by a contrastive alignment mechanism adapted from CLIP to guide multimodal visual features toward semantically meaningful language embeddings. This work contributes to the advancement of multimodal foundation models for remote sensing and offers a scalable way to integrate language understanding into geospatial analysis. We summarize our contribution as:

- We propose MMLGNet, a simple and effective framework that aligns heterogeneous remote sensing modalities like HSI and LiDAR along with the handcrafted textual descriptions using contrastive training, enabling semantically enriched feature representations in a shared latent space.
- We design the CNN-based encoders for HSI and LiDAR modalities, demonstrating that language supervision can effectively enhance visual representations without relying on complex architectures. Also, We perform visual-text contrastive alignment using prompts generated for land-cover classes,

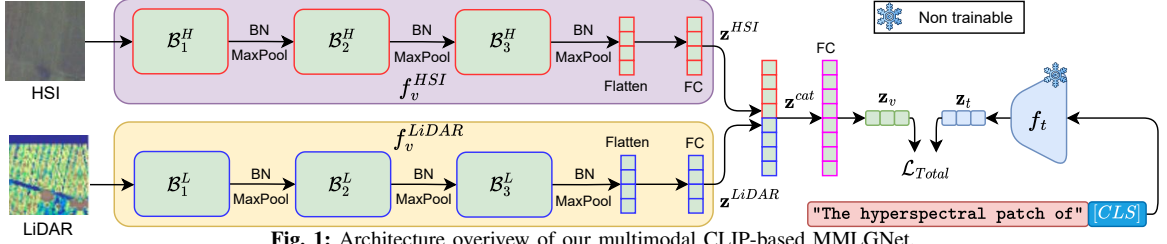


Fig. 1: Architecture overview of our multimodal CLIP-based MMLGNet.

bridging the semantic gap between raw visual features and natural language semantics.

- We evaluated our proposed MMLGNet on the MUUFL Gulfport and Trento datasets, where it consistently outperforms several established methods that rely solely on visual modalities.

II. METHODOLOGY

A. Preliminaries

Let us consider a multimodal RS dataset $\mathcal{D} = \{\mathbf{X}_{\text{HSI}}, \mathbf{X}_{\text{LiDAR}}, \mathbf{Y}\}$, where $\mathbf{X}_{\text{HSI}} \in \mathbb{R}^{H \times W \times B}$ represents the HSI with B spectral bands, $\mathbf{X}_{\text{LiDAR}} \in \mathbb{R}^{H \times W \times 1}$ denotes the corresponding registered LiDAR-derived elevation map, and $\mathbf{Y} \in \{1, 2, \dots, C\}^{H \times W}$ is the ground-truth label map with C semantic classes. Here, H and W denote the height and width of the spatial domain. To perform pixel-level classification, non-overlapping patches of size $P \times P$ are extracted from both modalities around each pixel, resulting in paired inputs: $\mathbf{p}^{\text{HSI}} \in \mathbb{R}^{B \times P \times P}$ and $\mathbf{p}^{\text{LiDAR}} \in \mathbb{R}^{1 \times P \times P}$. The goal is to learn a mapping function $\varphi_\theta : (\mathbf{p}^{\text{HSI}}, \mathbf{p}^{\text{LiDAR}}) \mapsto y$ that predicts the semantic label y for each pixel using the complementary spectral and structural information, with additional guidance from a language-based supervision framework.

B. Our proposed MMLGNet

Our proposed Multimodal Language-Guided Network (MMLGNet) is designed to learn a joint embedding space where semantically similar visual data from HSI and LiDAR sensors are aligned with natural language descriptions, shown in Figure 1. It comprises of modality-specific visual encoders parameterized by θ_v^H for HSI encoding and θ_v^L for LiDAR encoding, a fusion module, and a pretrained frozen text encoder f_t . The objective is to learn the parameters $\theta_v = \{\theta_v^H, \theta_v^L\}$ that maps the paired visual patches $(\mathbf{p}^{\text{HSI}}, \mathbf{p}^{\text{LiDAR}})$ to a visual embedding \mathbf{z}_v that is close to the text embedding \mathbf{z}_t of the corresponding ground-truth class description.

1) *Modality-Specific Visual Feature Extraction*: To process the heterogeneous inputs, we employ two specialized Convolutional Neural Networks (CNNs), an HSI encoder E_H and a LiDAR encoder E_L , which constitute our visual encoder backbone with parameters $\theta_v \in \{\theta_v^H, \theta_v^L\}$. Let a single convolutional block, \mathcal{B} , be defined as the composition of 2D convolution (*), Batch Normalization (BN), a non-linear activation function (σ), and Max Pooling. For an input feature map \mathbf{X} and learnable weights \mathbf{W} and bias \mathbf{b} , the operation is:

$$\mathcal{B}(\mathbf{X}; \mathbf{W}, \mathbf{b}) = \text{MaxPool}(\sigma(\text{BN}(\mathbf{X} * \mathbf{W} + \mathbf{b}))) \quad (1)$$

Given an HSI patch $\mathbf{x}_{\text{p}}^{\text{HSI}} \in \mathbb{R}^{B \times P \times P}$, the HSI encoder is a composition of three such convolutional blocks ($\mathcal{B}_1^H, \mathcal{B}_2^H, \mathcal{B}_3^H$), followed by a flatten operation and a fully connected (FC) layer i.e. linear layer. This process extracts a dense feature embedding, denoted in Equation 2, where the parameters θ_H consist of the weights and biases of the CNN and FC layers.

$$\mathbf{z}^{\text{HSI}} = \text{FC}(\text{Flatten}(\mathcal{B}_3^H(\mathcal{B}_2^H(\mathcal{B}_1^H(\mathbf{x}_{\text{p}}^{\text{HSI}}))))) \in \mathbb{R}^{D/2} \quad (2)$$

Similarly, for a LiDAR patch $\mathbf{p}^{\text{LiDAR}} \in \mathbb{R}^{1 \times P \times P}$, the LiDAR encoder E_L applies an analogous sequence of operations with its own set of parameters θ_L to produce a structural feature embedding defined in Equation 3.

$$\mathbf{z}^{\text{LiDAR}} = \text{FC}(\text{Flatten}(\mathcal{B}_3^L(\mathcal{B}_2^L(\mathcal{B}_1^L(\mathbf{p}^{\text{LiDAR}}))))) \in \mathbb{R}^{D/2} \quad (3)$$

2) *Multimodal Visual Feature Fusion*: The core of our network is an explicit fusion module that learns a joint representation from the individual modality features. The HSI and LiDAR feature embeddings are first concatenated to form a unified multimodal vector $\mathbf{z}^{\text{cat}} = \mathbf{z}^{\text{HSI}} \oplus \mathbf{z}^{\text{LiDAR}} \in \mathbb{R}^D$, where \oplus denotes the concatenation operation. The fused multimodal visual feature vector is then transformed by a linear fusion layer, parameterized by a weight matrix $\mathbf{w}_{\text{fuse}} \in \mathbb{R}^{D \times D}$ and bias $\mathbf{b}_{\text{fuse}} \in \mathbb{R}^D$. This layer projects the concatenated features into the final shared embedding space, producing the visual embedding $\mathbf{z}_v = \mathbf{w}_{\text{fuse}} \cdot \mathbf{z}^{\text{cat}} + \mathbf{b}_{\text{fuse}}$.

3) *Language-Vision Alignment*: We proposed to align the learnt visual embedding \mathbf{z}_v with a semantic text embedding \mathbf{z}_t using the pre-trained CLIP model's frozen text encoder. The encoder tokenises a text prompt t before feeding the tokens via a Transformer network. The final text embedding $\mathbf{z}_t \in \mathbb{R}^D$ is then obtained by linearly projecting the output embedding corresponding to the special '[EOT]' (End-of-Text) token. Also, to compute the contrastive loss between the multimodal visual embedding \mathbf{z}_v and the text embedding \mathbf{z}_t , we perform the L2-normalization represented as $\hat{\mathbf{z}}_v = \frac{\mathbf{z}_v}{\|\mathbf{z}_v\|_2}$ and $\hat{\mathbf{z}}_t = \frac{\mathbf{z}_t}{\|\mathbf{z}_t\|_2}$, respectively. These normalized vectors are used to compute the symmetric contrastive loss, which serves as the optimization objective for the learnable parameters θ_V and the fusion layer.

C. Network Optimization

Inspired from CLIP [11], we use the symmetric contrastive loss function to optimise the parameters of our MMLGNet, where we align the text and fused visual embeddings in the shared latent space. Consider a mini-batch of n image-text pairs, $\{(\mathbf{x}_{\mathbf{p}_i}, t_i)\}_{i=1}^n$, where \mathbf{p}_i represents

the pair of HSI and LiDAR patches for the i -th sample, and t_i is its corresponding text description such as "the hyperspectral patch of [CLS]". First, we compute a similarity matrix $\mathbf{S} \in \mathbb{R}^{n \times n}$, where each element $S_{ij} = \frac{\hat{\mathbf{z}}_{v,i} \cdot \hat{\mathbf{z}}_{t,j}^T}{\tau}$ represents the cosine similarity between the i -th visual embedding and the j -th text embedding, where, τ is a learnable temperature parameter that scales the logits, helping to control the sharpness of the distribution. Our goal is to maximize the similarity of the positive pairs while simultaneously minimizing the similarity of the negative pairs by reducing the symmetric cross-entropy loss over the similarity scores, defined in Equations 4 and 5.

-Visual-to-Text Loss ($\mathcal{L}_{v \rightarrow t}$) computes similarity and generate logits for a classification problem, where the goal is to predict the correct text for each visual input.

$$\mathcal{L}_{v \rightarrow t} = -\frac{1}{n} \sum_{i=1}^n \log \frac{\exp(S_{ii})}{\sum_{j=1}^n \exp(S_{ij})} \quad (4)$$

-Text-to-Visual Loss ($\mathcal{L}_{t \rightarrow v}$) predicts the appropriate visual input for every text prompt by treating each column of the similarity matrix (or each row of \mathbf{S}^T) as a logit.

$$\mathcal{L}_{t \rightarrow v} = -\frac{1}{n} \sum_{j=1}^n \log \frac{\exp(S_{jj})}{\sum_{i=1}^n \exp(S_{ij})} \quad (5)$$

The final optimization objective is the average of these two losses $\mathcal{L}_{\text{total}} = \frac{\mathcal{L}_{v \rightarrow t} + \mathcal{L}_{t \rightarrow v}}{2}$, ensuring a robust, bidirectional alignment between the modalities, defined in Equation 6.

$$\psi_{\theta}^* = \arg \min_{\psi_{\theta}} \mathcal{L}_{\text{total}} \quad (6)$$

III. EXPERIMENTAL EVALUATIONS

Dataset description: We experiment our proposed MMLGNet with two benchmark multimodal remote sensing datasets. a) **MUUFL Gulfport** [15] dataset is acquired over the University of Southern Mississippi contains a 325×220 pixel hyperspectral imaging (HSI) with 64 post-processed spectral bands. It also includes LiDAR elevation data from two rasters and covers 11 urban land-cover classes with 1100 training and 52587 testing samples. b) **Trento** dataset was acquired over rural areas south of Trento, Italy, which consists of 63 HSI bands [16]. The LiDAR provides a single elevation raster. The 600×166 -pixel scene includes six mutually exclusive vegetation classes. For our experiments, we used the standard disjoint training and test sets provided with the dataset, which consist of 600 training and 29,614 testing samples. We extract the patch of size 11x11 for all the experiments.

Architecture details: The proposed MMLGNet employs two modality-specific vision encoders for HSI and LiDAR data, each processing 11×11 input patches and projecting them into a shared 512-dimensional embedding space. The HSI encoder takes an $11 \times 11 \times B$ patch (where $B = 63$ for Trento and $B = 64$ for MUUFL) and passes it through three convolutional stages. Firstly, we use 64 filters of size 3×3 , followed by batch normalization, ReLU activation, and 2×2 max-pooling, reducing the spatial size from 11×11 to 5×5 . Thereafter we

TABLE I: Accuracy analysis on the Trento dataset (in %).

Classes	SVM [17]	ELM [18]	TB-CNN [19]	FusAtNet [20]	MMLGNet
Apples	85.49	95.81	98.07	98.99	99.95
Buildings	89.76	96.97	95.21	99.31	99.68
Ground	59.56	96.66	93.32	95.87	100.00
Woods	97.42	99.39	99.93	99.93	99.89
Vineyard	93.85	82.24	98.78	99.56	99.81
Roads	89.96	86.52	89.98	91.23	95.74
OA	92.30	91.32	97.92	99.06	99.42
AA	86.01	92.93	96.19	98.48	99.18
κ	0.8971	0.9042	0.9681	0.9879	0.9922

TABLE II: Performance comparison on the MUUFL Gulfport dataset (in %).

Classes	SVM [17]	ELM [18]	TB CNN [19]	FusAtNet [20]	MMLGNet
Trees	95.97	94.89	97.40	98.10	89.97
Grass Pure	62.71	62.23	76.84	71.66	86.67
Grass Ground Surface	83.60	83.15	84.31	87.65	77.07
Dirt and Sand	78.60	57.88	84.93	86.42	98.32
Road Materials	92.72	93.33	93.41	95.09	90.80
Water	95.10	68.32	10.78	90.73	99.18
Buildings' Shadow	71.23	47.01	63.34	74.27	93.53
Buildings	87.96	77.58	96.20	97.55	94.20
Sidewalk	41.11	32.15	54.30	60.44	76.58
Yellow Curb	11.05	0.00	2.21	9.39	93.98
Cloth Panels	88.76	78.29	87.21	93.02	99.41
OA	86.90	83.10	89.38	91.48	88.79
AA	83.37	63.17	68.26	78.58	90.87
κ	0.8255	0.7742	0.8583	0.8865	0.8542

apply 128 filters and further reduces it to 2×2 , while the final block uses 256 filters to reach 1×1 . The output is flattened and passed through a fully connected layer, resulting in an HSI embedding $\mathbf{z}^{\text{HSI}} \in \mathbb{R}^{256}$.

Similarly, the LiDAR encoder processes an $11 \times 11 \times 1$ DSM patch through three convolutional stages: 32, 64, and 128 filters, respectively, each followed by 2×2 max-pooling to obtain a 1×1 feature map. This is flattened and passed through a fully connected layer to produce a 256-dimensional LiDAR embedding $\mathbf{z}^{\text{LiDAR}} \in \mathbb{R}^{256}$. These two modality-specific embeddings are concatenated and passed through a linear layer to form the final visual embedding $\mathbf{z}_v \in \mathbb{R}^{512}$. This embedding is L2-normalized and optimized using contrastive loss against the corresponding text embedding $\mathbf{z}_t \in \mathbb{R}^{512}$, obtained from a frozen pretrained CLIP text encoder f_t [11].

Training and evaluation protocols: We perform all the experiments using on T4 GPU provided by Google Colab(free tier) with Pytorch deep learning framework. The proposed MMLGNet has been optimized using the Adam optimizer [21] with a learning rate of 1×10^{-4} for maximum of 100 epochs with a batch size of 128. Also, we employed an early stopping mechanism with a patience of 15 epochs to avoid overfitting. The best-performing model has been evaluated on the test set using three standard metrics: Overall Accuracy (OA), Average Accuracy (AA), and the Cohen's Kappa coefficient (κ).

A. Comparison to Literature

We compare the proposed MMLGNet against outperforms several established methods that rely solely on visual modalities using the Trento and MUUFL Gulfport datasets. It is important to note that the primary goal of our proposed MMLGNet is to showcase the advantage of leveraging multimodal

TABLE III: Ablation study on the loss function components.

Loss	Trento			MUUFL		
	OA	AA	κ	OA	AA	κ
$\mathcal{L}_{t \rightarrow v}$	99.26	98.91	0.9901	88.51	90.16	0.8499
$\mathcal{L}_{v \rightarrow t}$	99.27	98.98	0.9902	88.32	90.31	0.8478
$\mathcal{L}_{v \rightarrow t} + \mathcal{L}_{t \rightarrow v}$	99.42	99.18	0.9922	88.79	90.87	0.8542

TABLE IV: Performance comparison with different text encoders.

Text Encoder	Trento			MUUFL		
	OA	AA	κ	OA	AA	κ
BERT Base	99.36	99.01	0.9914	86.47	88.52	0.8240
RoBERTa Base	99.48	99.19	0.9931	86.37	88.96	0.8235
ALBERT Base-v2	99.35	98.98	0.9913	87.17	89.71	0.8338
CLIP RN50	99.32	98.98	0.9909	88.29	90.40	0.8475
CLIP ViT-B/16	99.31	98.90	0.9908	88.03	89.40	0.8436
CLIP ViT-B/32	99.42	99.18	0.9922	88.79	90.87	0.8542

information by integrating remote sensing visual data with language modality. Specifically, on the Trento dataset, MMLGNet surpasses SVM [17], ELM [18], Two-branch(TB-CNN) [19], and FusAtNet [20] as shown in Table I. We further evaluate MMLGNet on the MUUFL Gulfport dataset, where it achieves a substantial gain in AA, outperforming referred methods by a margin of at least 12%. These results signifies the effectiveness of incorporating language-guided information for improved generalization and semantic alignment in multimodal RS.

B. Ablation Studies

Ablation with loss functions: As defined in Equation 6, the symmetric contrastive loss jointly optimizes visual-to-text ($\mathcal{L}_{v \rightarrow t}$) and text-to-visual ($\mathcal{L}_{t \rightarrow v}$) alignments. We ablate MMLGNet by training with each loss individually and compare the results with the full bi-directional loss, as shown in Table III. The symmetric loss consistently yields the best performance, improving average accuracy by 0.16% on Trento and 0.22% on MUUFL over $\mathcal{L}_{t \rightarrow v}$, and by 0.15% and 0.47% over $\mathcal{L}_{v \rightarrow t}$ on Trento and MUUFL, respectively.

Comparison with Different Text Encoders: In Table IV, we ablate with different text encoder backbones on the performance of the proposed MMLGNet. Specifically, we experiment with six pretrained and frozen text encoders: BERT-base[22], RoBERTa-base[23], ALBERT-base-v2[24], CLIP RN50, CLIP ViT-B/16, and CLIP ViT-B/32. Our results show that RoBERTa-base and CLIP ViT-B/32 are more effective in aligning multimodal visual features compared to other text encoders, achieving superior performance of at least 0.06% and 0.5% for Trento and MUUFL Gulfport datasets, respectively.

Ablation for multimodal visual features: To quantify and demonstrate the effectiveness of our fusion strategy, we perform ablation on our MMLGNet architecture using three configurations HSI, LiDAR and HSI+LiDAR. Table V presents the performance comparison, where we observe that the multimodal visual features guided by language modality outperform the individual visual modality settings in AA by 9.42% and 28.65% for Trento and MUUFL datasets, respectively.

Impact of LiDAR channels: We analyze the sensitivity of MMLGNet for LiDAR modality by varying the number of LiDAR input channels i.e., digital surface model (DSM) and digital terrain model (DTM). We experimented using DSM,

TABLE V: Architecture ablation study on Trento and MUUFL datasets.

Modality	Trento			MUUFL		
	OA	AA	κ	OA	AA	κ
HSI	93.58	89.76	0.9140	56.90	61.98	0.4832
LiDAR	42.30	38.84	0.3066	14.84	25.99	0.0904
HSI+LiDAR	99.42	99.18	0.9922	88.79	90.87	0.8542

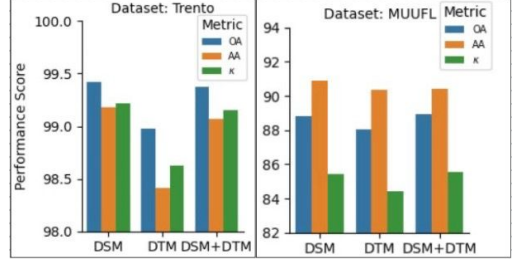


Fig. 2: Ablation study on the LiDAR input channels.

DTM and DSM + DTM. We found that DTM + DSM setting slightly outperforms OA by 0.05% in Trento dataset, whereas for MUUFL dataset, DTM + DSM performs better than DSM on OA by 0.17%, shown in Figure 2.

Output classification maps: In Figure 3, we showcase the output classification maps generated from our proposed MMLGNet in the a) Trento and b) MUUFL datasets, which clearly demonstrates the class mappings learned under the language-guided multimodal setup.

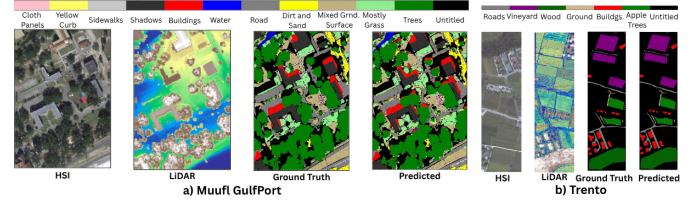


Fig. 3: Classification maps for HSI, LiDAR, ground truth, and MMLGNet predictions on (a) MUUFL and (b) Trento datasets.

IV. CONCLUSION AND FUTURE WORK

The primary goal of this work is to demonstrate the value of integrating textual supervision into multimodal remote sensing (RS) using a simple CNN-based visual architecture. To achieve this, we proposed MMLGNet, a simple framework that aligns visual features from HSI and LiDAR with textual embeddings through contrastive learning. Inspired by CLIP, our method optimizes modality-specific visual features against handcrafted text prompts, enabling semantically rich and unified representations. We evaluate MMLGNet on two benchmark multimodal RS datasets, where it consistently outperforms several methods and improves interpretability. Through modality-aware encoders and contrastive alignment, MMLGNet effectively bridges the semantic gap across modalities. Our ablation studies further validate the importance of textual guidance in enhancing performance. In future, our goal is to go beyond manually made prompts and look into prompt learning methods, which could improve performance and adaptability even more.

REFERENCES

[1] W. Li, E. W. Tramel, S. Prasad, and J. E. Fowler, "Nearest regularized subspace for hyperspectral classification," *IEEE Transactions on Geoscience and Remote Sensing*, vol. 52, no. 1, pp. 477–489, 2014.

[2] L.-Z. Huo, C. A. Silva, C. Klauberg, M. Mohan, L.-J. Zhao, P. Tang, and A. T. Hudak, "Supervised spatial classification of multispectral lidar data in urban areas," *PLOS ONE*, vol. 13, no. 10, p. e0206185, Oct. 2018. [Online]. Available: <http://dx.doi.org/10.1371/journal.pone.0206185>

[3] B. Koetz, F. Morsdorf, S. Van der Linden, T. Curt, and B. Allgöwer, "Multi-source land cover classification for forest fire management based on imaging spectrometry and lidar data," *Forest Ecology and Management*, vol. 256, no. 3, pp. 263–271, 2008.

[4] N. Kussul, M. Lavreniuk, S. Skakun, and A. Shelestov, "Deep learning classification of land cover and crop types using remote sensing data," *IEEE Geoscience and Remote Sensing Letters*, vol. 14, no. 5, pp. 778–782, 2017.

[5] Q. Yuan, H. Shen, T. Li, Z. Li, S. Li, Y. Jiang, H. Xu, W. Tan, Q. Yang, J. Wang *et al.*, "Deep learning in environmental remote sensing: Achievements and challenges," *Remote sensing of Environment*, vol. 241, p. 111716, 2020.

[6] P. Shu, R. W. Aslam, I. Naz, B. Ghaffar, D. E. Kucher, A. Quddoos, D. Raza, M. Abdullah-Al-Wadud, and R. M. Zulqarnain, "Deep learning-based super-resolution of remote sensing images for enhanced groundwater quality assessment and environmental monitoring in urban areas," *IEEE Journal of Selected Topics in Applied Earth Observations and Remote Sensing*, 2025.

[7] S. P. Healey, W. B. Cohen, Z. Yang, C. K. Brewer, E. B. Brooks, N. Gorelick, A. J. Hernandez, C. Huang, M. J. Hughes, R. E. Kennedy *et al.*, "Mapping forest change using stacked generalization: An ensemble approach," *Remote Sensing of Environment*, vol. 204, pp. 717–728, 2018.

[8] S. Chaib, H. Liu, Y. Gu, and H. Yao, "Deep feature fusion for vhr remote sensing scene classification," *IEEE Transactions on Geoscience and Remote Sensing*, vol. 55, no. 8, pp. 4775–4784, 2017.

[9] A. Jha, S. Bose, and B. Banerjee, "Gaf-net: Improving the performance of remote sensing image fusion using novel global self and cross attention learning," in *Proceedings of the IEEE/CVF Winter Conference on Applications of Computer Vision (WACV)*, January 2023, pp. 6354–6363.

[10] H. Shen, Y. Lin, Q. Tian, K. Xu, and J. Jiao, "A comparison of multiple classifier combinations using different voting-weights for remote sensing image classification," *International journal of remote sensing*, vol. 39, no. 11, pp. 3705–3722, 2018.

[11] A. Radford, J. W. Kim, C. Hallacy, A. Ramesh, G. Goh, S. Agarwal, G. Sastry, A. Askell, P. Mishkin, J. Clark *et al.*, "Learning transferable visual models from natural language supervision," in *International conference on machine learning*. PMLR, 2021, pp. 8748–8763.

[12] J. Deng, W. Dong, R. Socher, L.-J. Li, K. Li, and L. Fei-Fei, "Imagenet: A large-scale hierarchical image database," in *2009 IEEE conference on computer vision and pattern recognition*. Ieee, 2009, pp. 248–255.

[13] M. Singha, A. Jha, B. Solanki, S. Bose, and B. Banerjee, "Applenet: Visual attention parameterized prompt learning for few-shot remote sensing image generalization using clip," in *Proceedings of the IEEE/CVF Conference on Computer Vision and Pattern Recognition (CVPR) Workshops*, June 2023, pp. 2024–2034.

[14] V. Vivanco Cepeda, G. K. Nayak, and M. Shah, "Geoclip: Clip-inspired alignment between locations and images for effective worldwide geo-localization," *Advances in Neural Information Processing Systems*, vol. 36, pp. 8690–8701, 2023.

[15] X. Du and A. Zare, "Technical Report: Scene Label Ground Truth Map for MUUFL Gulfport Data Set," University of Florida, Gainesville, FL, Tech. Rep. 20170417, Apr. 2017. [Online]. Available: <http://ufdc.ufl.edu/IR00009711/00001>

[16] tyust-dayu, "Trento Dataset: Hyperspectral Image and LiDAR Data," <https://github.com/tyust-dayu/Trento/tree/b4afc449ce5d6936ddc04fe267d86f9f35536afd>, accessed: 2025-06-14.

[17] G. Mercier and M. Lennon, "Support vector machines for hyperspectral image classification with spectral-based kernels," in *International Geoscience and Remote Sensing Symposium (IGARSS)*, vol. 1, 08 2003, pp. 288 – 290 vol.1.

[18] W. Li, C. Chen, H. Su, and Q. Du, "Local binary patterns and extreme learning machine for hyperspectral imagery classification," *IEEE Transactions on Geoscience and Remote Sensing*, vol. 53, no. 7, pp. 3681–3693, 2015.

[19] X. Xiaodong, L. Wei, R. Qiong, D. Qian, G. Lianru, and Z. Bing, "Multisource remote sensing data classification based on convolutional neural network," *IEEE Transactions on Geoscience and Remote Sensing*, vol. 56, no. 2, pp. 937–949, 02 2018. [Online]. Available: <https://cir.nii.ac.jp/crid/1363107368333204480>

[20] S. Mohla, S. Pande, B. Banerjee, and S. Chaudhuri, "Fusatnet: Dual attention based spectrospatial multimodal fusion network for hyperspectral and lidar classification," in *2020 IEEE/CVF Conference on Computer Vision and Pattern Recognition Workshops (CVPRW)*, 2020, pp. 416–425.

[21] D. P. Kingma and J. Ba, "Adam: A method for stochastic optimization," 2017. [Online]. Available: <https://arxiv.org/abs/1412.6980>

[22] J. Devlin, M. Chang, K. Lee, and K. Toutanova, "BERT: pre-training of deep bidirectional transformers for language understanding," *CoRR*, vol. abs/1810.04805, 2018. [Online]. Available: <http://arxiv.org/abs/1810.04805>

[23] Y. Liu, M. Ott, N. Goyal, J. Du, M. Joshi, D. Chen, O. Levy, M. Lewis, L. Zettlemoyer, and V. Stoyanov, "Roberta: A robustly optimized BERT pretraining approach," *CoRR*, vol. abs/1907.11692, 2019. [Online]. Available: <http://arxiv.org/abs/1907.11692>

[24] Z. Lan, M. Chen, S. Goodman, K. Gimpel, P. Sharma, and R. Soricut, "ALBERT: A lite BERT for self-supervised learning of language representations," *CoRR*, vol. abs/1909.11942, 2019. [Online]. Available: <http://arxiv.org/abs/1909.11942>